Fluctuating auxin response gradients determine pavement cell-shape acquisition

Peter Grones[a,b,c], Mateusz Majda[a,1], Siamsa M. Doyle[a], Daniël Van Damme[b,c], and Stéphanie Robert[a,2]

[a]Umeå Plant Science Centre, Department of Forest Genetics and Plant Physiology, Swedish University of Agricultural Sciences, 901 83 Umeå, Sweden; [b]Department of Plant Biotechnology and Bioinformatics, Ghent University, 9052 Ghent, Belgium; and [c]VIB Center for Plant Systems Biology, Ghent University, 9052 Ghent, Belgium

Puzzle-shaped pavement cells provide a powerful model system to investigate the cellular and subcellular processes underlying complex cell-shape determination in plants. To better understand pavement cell-shape acquisition and the role of auxin in this process, we focused on the spirals of young stomatal lineage ground cells of *Arabidopsis* leaf epidermis. The predictability of lobe formation in these cells allowed us to demonstrate that the auxin response gradient forms within the cells of the spiral and fluctuates based on the particular stage of lobe development. We revealed that specific localization of auxin transporters at the different membranes of these young cells changes during the course of lobe formation, suggesting that these fluctuating auxin response gradients are orchestrated via auxin transport to control lobe formation and determine pavement cell shape.

Arabidopsis | pavement cells | auxin response gradient | auxin transporter | lobe formation

The leaf epidermis is an important architectural control element that regulates the growth of underlying tissues and the overall form of the organ. In *Arabidopsis thaliana*, the anticlinal walls of the pavement cells in the leaf epidermis are undulated and create the impression of a jigsaw puzzle-like pattern, since neighboring cells perfectly interdigitate with each other. Due to their interdigitated shape requiring synchronized growth regulation, pavement cells in particular offer a unique system to improve our understanding of how plant cells reach their final morphology. In order to better understand cell-shape acquisition, we took advantage of the developmental synchrony of a subpopulation of leaf epidermal pavement cells, stomatal lineage ground cells (SLGCs), found in anisocytic stomatal complexes. These cells are produced during asymmetrical division of meristemoid cells, which can divide three consecutive times, producing up to three monoclonal SLGCs before differentiating into a guard mother cell and stoma (Fig. 1 *A* and *B*) (1, 2).

Results and Discussion

Pavement Cell First Lobe Formation Is Orchestrated in a Systematic and Synchronous Manner.
We focused our analyses on first-lobe formation in the youngest of the SLGCs, which are always positioned beside a meristemoid or stoma (SLGC 1 in Fig. 1 *A* and *B*). We observed that the youngest SLGC (SLGC 1 in Fig. 1*C*) systematically forms its first lobe into an older neighboring cell at the membrane/wall unit that is positioned opposite the neighboring stoma (SLGC 2 in Fig. 1*C*). We quantified the outgrowth angle of the first lobe (defined as an outgrowth ratio of greater than 1,1 or 10%; *Materials and Methods*) of the youngest SLGCs (as an example, see SLGC 2 in Fig. 1*C*) with respect to the position of the neighboring stoma. All first-lobe outgrowths occurred approximately perpendicular to the position of the stoma (Fig. 1*D*).

This system allowed us to predict rather accurately where the first lobe of a nonlobed SLGC would form and thus directly focus on lobe initiation. We took advantage of this synchronous system of lobe development to investigate the role of auxin in first-lobe formation in pavement cells.

Auxin Regulates Pavement Cell-Lobe Formation in a Dose-Dependent Manner.
Previous studies suggest that pavement cell-lobe acquisition is tightly regulated by auxin (3–5). Therefore, we quantitatively analyzed the size and shape of pavement cells of the auxin overproduction mutant *yuc1D*, in which the *YUC1* gene is driven by the 35S promoter. Both the size and lobe number of pavement cells were increased in *yuc1D* compared with the wild type (*SI Appendix*, Fig. S1 *A* and *B*). Moreover, we investigated the size and shape of pavement cells in wild-type plants exposed to different concentrations of 1-naphthaleneacetic acetic acid (NAA) and indole-3-acetic acid (IAA), revealing dose-dependent effects of the treatments (*SI Appendix*, Fig. S1 *C–F*). Our results suggest that both pavement cell size and lobe formation are dose-dependently regulated by auxin. These findings reveal an analogous dose-dependent nature of auxin regulation of pavement cell development to that which has previously been identified for many other developmental processes, such as primary root growth, root hair growth, initiation of lateral root primordia, or root cap self-renewal (6–10).

Auxin activity is mainly transcribed through the nuclear auxin signaling pathway composed of the F box-containing TRANSPORT INHIBITOR RESISTANT1/AUXIN SIGNALING F BOX (TIR1/AFB) proteins, the transcriptional corepressors AUXIN/INDOLE-3-ACETIC ACID (Aux/IAA), and the AUXIN RESPONSE FACTOR transcription factors (11). We analyzed the size and shape of pavement cells in different *tir1/afb* mutants

---

Significance

As the outermost cell layer of an organism, the epidermis plays a key role in controlling morphogenesis. In this work, we investigated cell-shape regulation in young, lobing pavement cells of the *Arabidopsis* leaf epidermis. By taking advantage of their developmental synchrony, we showed that the establishment of a local auxin gradient is necessary for the initiation of first-lobe formation. However, the auxin gradient is not stable over time but rather fluctuates according to the particular developmental stage of the cells. These changes are established by the specific distribution of auxin transporters at the different membranes of these young pavement cells. This work reports an observation of auxin fluctuation during cell-shape determination in plants.
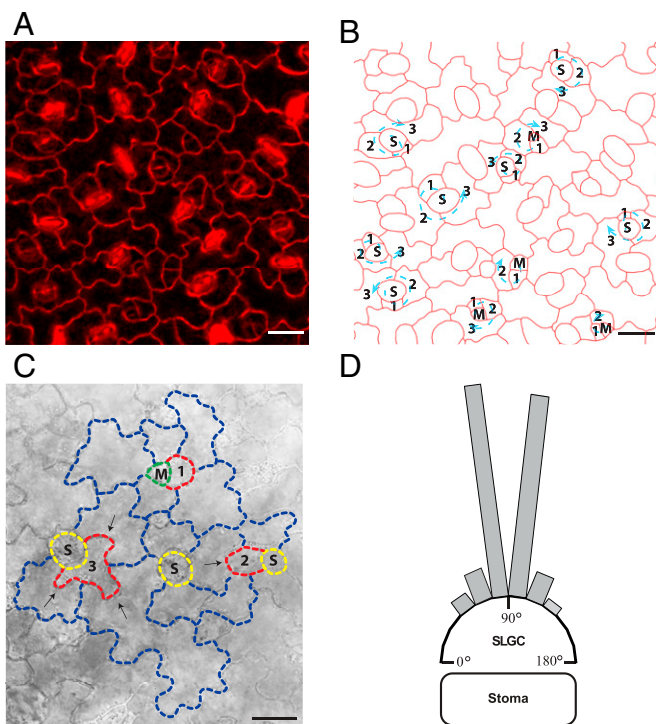
PLANT BIOLOGY

Fig. 1. SLGCs are the ideal system to study cell-shape acquisition. (*A*) Image of pavement cells from the third leaf of *Arabidopsis* (cell walls are stained with propidium iodide). (*B*) Outlines of the cells in the image from *A* with marked spiral patterning originating from asymmetric divisions of meristemoid cells. Numbers mark the cell stage in the spiral from the youngest (*1*) to the oldest (*3*) and arrows mark the clockwise or counterclockwise direction of the spiral. M, meristemoid; S, stoma. (*C*) Asymmetric division of the meristemoid cell produces a new meristemoid cell and an SLGC (*1*). During growth and development, the SLGC (*2*) always produces its first lobe (marked with an arrow) into an older neighboring cell. Example of an older SLGC (*3*) forming three lobes (marked with arrows) into older neighboring cells. (*D*) Position of first-lobe outgrowth in SLGCs. In these cells the vast majority of lobe outgrowth occurs opposite the stoma. Each bar represents the proportion of analyzed lobes for which outgrowth occurred in the indicated 15° angle range. Angles were measured from the lobe outgrowth to the center of the neighboring stoma. *n* = 47 lobes. (Scale bars, 20 μm.)

treated with a low NAA concentration (20 nM). While *tir1/afb1/afb2* and *afb4/afb5* mutants exhibited increased cell area similar to the wild type after auxin treatment, *tir1* and *afb1/afb2* mutants exhibited decreased cell area (*SI Appendix*, Fig. S2 *A* and *C*). Only the *afb4/afb5* mutant showed an auxin-induced increase in lobe number as observed in the wild type, whereas lobe number in all of the other mutants was insensitive to auxin treatment (*SI Appendix*, Fig. S2 *B* and *C*). These data suggest that fluctuating auxin levels during lobe acquisition might trigger formation of different combinations of TIR1/AFB and Aux/IAA coreceptor complexes with a wide range of auxin-binding affinities, which lead to specific response outputs (12–14).

Auxin Response Gradients within Anisocytic Complexes Play a Role in Regulating Lobe Formation. To further dissect the role of auxin in lobe formation, we examined the distribution of the auxin signaling reporter DR5::Venus-NLS (nuclear localization signal) (15) in the leaf epidermal plane. The presence of nuclearly localized DR5 signal was observed in almost every pavement cell (*SI Appendix*, Fig. S3*A*), suggesting that intracellular auxin is present throughout the different stages of pavement cell growth and development. The expression of the auxin-responsive promoter DR5 has been used as a proxy for auxin concentration in

several tissues such as the root meristem, shoot apical meristem, and lateral root founder cells (15–18). In many cases, this assumption has been confirmed by the observation of the more direct DII-Venus reporter (19–21). It is therefore most likely that DR5 expression directly correlates with auxin concentration in pavement cells as well. The permanent presence of auxin, however, hindered us from using DII-Venus, as no DII signals could be observed in the pavement cells. We next focused on DR5 signals specifically within the spirals of anisocytic stomatal complexes. In order to analyze auxin response during lobe formation, we divided the spiral anisocytic complexes into three groups, corresponding to three developmental stages (Fig. 2*A*): 1) nonlobed youngest SLGC next to a meristemoid; 2) nonlobed youngest SLGC next to a stoma; and 3) lobed youngest SLGC next to a stoma.

As observed previously (22), just after asymmetric division of the meristemoid, DR5 signal levels were similar in both newly formed cells—the new meristemoid and the youngest SLGC (Fig. 2*B*). Ultimately, after a series of asymmetric divisions, the meristemoid transitions into a guard mother cell and consequently divides symmetrically to form two guard cells (Fig. 2*A*). As has been shown previously (22), this is accompanied by a decrease in auxin reporter signal intensity in the guard mother cell, suggesting auxin deprivation (Fig. 2*C*). Remarkably, when we closely analyzed DR5 signal throughout the individual cells of the stomatal complexes, we discovered a gradient of auxin response within the spirals. In stage 1 complexes, the DR5 signal usually increased with increasing cell age within the cells of the spirals, with the weakest signal in the meristemoid cell (youngest) and strongest in the largest (oldest) cell (Fig. 2*D*), and this was the case in 85% of stage 1 spirals (Fig. 2 *D* and *H*). For stage 2 spirals, we observed a similar ascending DR5 signal gradient in 82% of cases (Fig. 2 *E* and *H*). However, by stage 3, once the first lobe was formed, the occurrence of such an ascending DR5 signal gradient had reduced to only 46% of cases (Fig. 2 *F* and *H*), suggesting that lobe development in the youngest SLGCs may coincide with a change in auxin response distribution within the cells of the spirals. In contrast, 35% of the cells in the spirals in stage 3 exhibited a descending DR5 signal gradient, with the highest DR5 signal found in the youngest, now lobed, SLGC (Fig. 2*G*). We next investigated the possible correlation between DR5 intensity and cell area or developmental stage of SLGCs. However, within the same leaf, we could observe SLGCs at the same developmental stage with similar cell area but different DR5 signal intensity and vice versa (*SI Appendix*, Fig. S3*B*), strongly arguing against such a correlation. Overall, these results agree with our findings of dose-dependent auxin regulation of cell growth and lobe formation. Lobing is not just a consequence of cell growth, but cell growth and lobing are connected and regulated in auxin-dependent manner. There are several examples of mutants such as *CA-rop2* and *any1* that exhibit cellular growth without lobing (23, 24). On the other hand, *mur3-1* mutants exhibit bigger pavement cells, but fewer lobes per cell, than the wild type (25).

Our results suggest that establishment of a low auxin response in the youngest SLGC of anisocytic complexes is linked with first-lobe formation in this cell. Additionally, our data indicate that the auxin response level in SLGCs is not constant throughout development but rather dynamically changes during the formation of the first lobe. Analogous dynamic fluctuations of auxin concentrations, orchestrated by active cellular transport rather than auxin biosynthesis, have been described during phyllotaxis (26–28). Moreover, similar dynamic fluctuations in auxin levels, as indicated by DR5 expression, as well as oscillating auxin-responsive gene expression, have been observed during lateral root initiation (17, 18, 29) but have not been previously shown to play a role in cell-shape regulation.
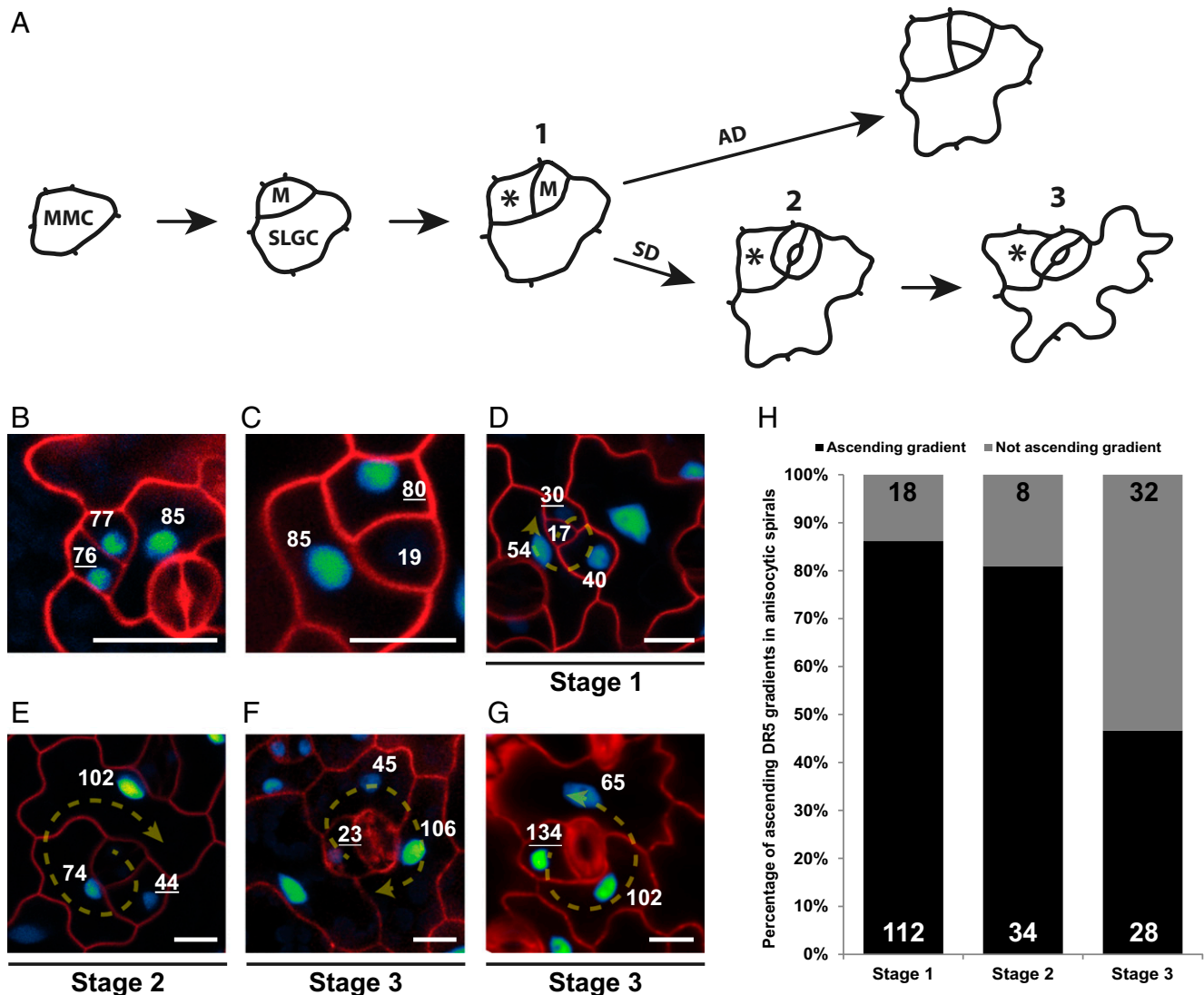
Fig. 2. Ascending auxin response gradient within the spirals of stomatal complexes. (*A*) Scheme representing the fate of a meristemoid cell, which can undergo either an asymmetric (AD) or symmetric (SD) division to produce an SLGC or stomatal guard cells, respectively. Numbers represent three different stages into which the spiral complexes were divided: 1) nonlobed youngest SLGC next to a meristemoid; 2) nonlobed youngest SLGC next to a stoma; and 3) lobed youngest SLGC next to a stoma. Asterisks mark the youngest SLGC in each stage. MMC, meristemoid mother cell. (*B*) DR5::Venus-NLS expression is similar in the newly formed meristemoid and SLGC after an asymmetric division. (*C*) Depletion of the DR5::Venus-NLS signal from the guard mother cell before a symmetric division. (*D–F*) Representative images of DR5::Venus-NLS signal distribution within anisocytic stomatal complexes at the different stages shown in *A*. The directions of the spiral division patterns are shown by arrows. (*G*) Example of a descending youngest-to-oldest DR5 signal gradient, with the youngest SLGC exhibiting highest DR5::Venus-NLS signal distribution within a single anisocytic spiral. The direction of the spiral division pattern is shown by an arrow. (*B–G*) Cell walls are stained with propidium iodide. Numbers represent quantified DR5 fluorescence signal intensity in the nucleus. Underlined numbers mark the youngest SLGC. (Scale bars, 10 μm.) (*H*) Quantification of the frequency of ascending DR5 signal distribution gradients from youngest to oldest cells within anisocytic stomatal complexes at the different stages shown in *A*; *n* values are displayed in the graph.

Auxin Transport Rather than Biosynthesis Contributes to Auxin Response Gradient Formation in the Anisocytic Spiral Complexes. Our results suggest that auxin response gradients, which are known to be crucial for coordinating the patterning of organs (16, 30, 31), might also play a role in pavement cell-shape acquisition. Auxin gradients could potentially be generated by local auxin biosynthesis and/or polar auxin transport. We therefore investigated the potential role of auxin biosynthesis in auxin gradient formation within young developing leaves, which have been shown to be the main sites of auxin production in *Arabidopsis* (32). We analyzed the DR5 signal distribution within the spirals of anisocytic stomatal complexes of the auxin overproduction mutant *yuc1D*. The distribution of ascending compared with nonascending DR5 gradients within the spirals was similar in *yuc1D* and wild type (Fig. 3*A*). This suggests

that auxin biosynthesis might not be the direct process influencing auxin gradient establishment within the anisocytic spirals. Besides auxin biosynthesis, several other processes such as auxin catabolism, conjugation, or transport have also been shown to participate in the regulation of cellular auxin concentration (33).

To address the potential role of auxin transport during the lobe-formation process, we focused on one mutant deficient in PIN-FORMED (PIN) auxin exporters (*pin3/4/7*) (34), one deficient in AUXIN-RESISTANT1 (AUX1)/LIKE AUX1 (AUX/LAX) auxin importers (*aux1*) (35–37), and two deficient in ATP-binding cassette protein subfamily B (ABCB) auxin exporters (*abcb1*, *abcb19*) (38–41), for which most of the affected genes have previously been shown to be expressed in leaves (22, 38, 42, 43). Remarkably, all of the mutants analyzed exhibited a strong
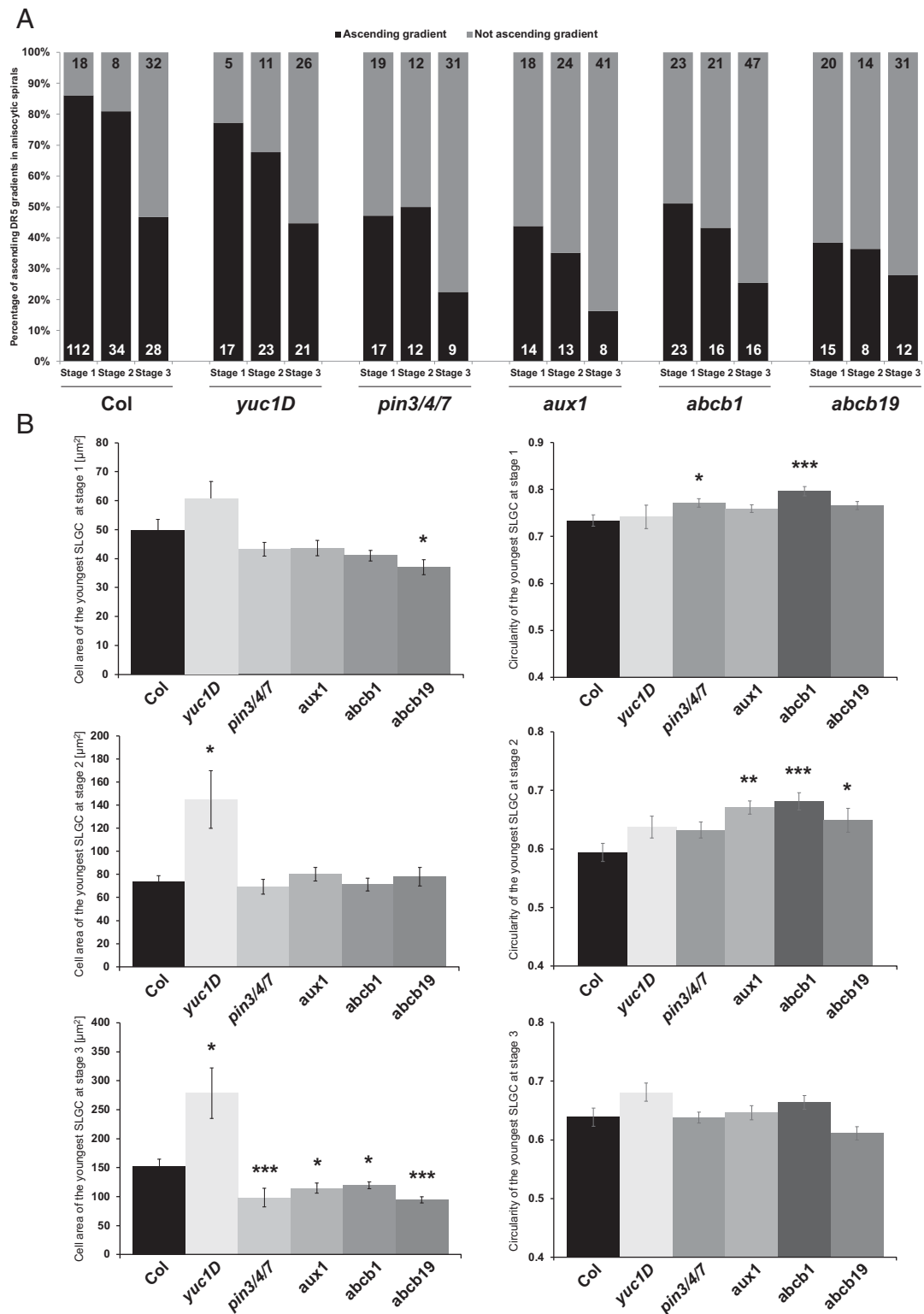
Fig. 3. Auxin transport mutants reveal defects in auxin reporter distribution in anisocytic stomatal spirals. (*A*) Quantification of the frequency of ascending DR5::Venus-NLS signal distribution gradients from youngest to oldest cells within anisocytic stomatal complexes at the different stages (shown in Fig. 2*A*) in Col, *yuc1D*, *aux1*, *abcb1*, *abcb19*, and *pin3/4/7* mutants. *n* values are displayed in the graphs. (*B*) Cell area and circularity quantification of the youngest SLGCs from the anisocytic stomatal complexes of the mutants at stage 1, 2, or 3. Asterisks on the schemes mark the youngest SLGCs, on which the quantifications were performed. Error bars correspond to ±SE. Statistical significance compared with the Columbia wild type was tested by Wilcoxon test (*$P < 0.05$, **$P < 0.01$, ***$P < 0.001$).

decrease in the occurrence of ascending youngest-to-oldest cell DR5 signal gradient patterns within the spirals in all three stages (Fig. 3*A*), compared with that found for wild type. Our results therefore strongly suggest that the establishment of an auxin gradient in the anisocytic spirals is driven by auxin transport.

Auxin has been shown to play an important role in lobe formation as it stimulates the asymmetric distribution of PIN proteins, regulators of local auxin accumulation (3, 44, 45). Therefore, we evaluated the cell area and shape of the youngest SLGCs within the spirals of the *yuc1D* auxin biosynthesis mutant and *pin3/4/7*, *aux1*, *abcb1*, and *abcb19* auxin transporter mutants. We observed a significant increase in the cell area of the *yuc1D* mutant at stages 2 and 3 compared with the wild type. However, the auxin transport mutants exhibited a significant decrease of cell area preferentially at stage 3 (Fig. 3*B*). This would suggest that an increased and stable concentration of auxin induces growth, as we observed with exogenous auxin treatment (*SI Appendix*, Fig. S1). Since it would make little sense to measure the lobe number in the youngest SLGCs from the spirals, we focused on circularity, which was shown previously to correlate with changes in lobe number during pavement cell development (25). We observed significant changes in the circularity of the youngest SLGCs in auxin transporter mutants, but not in the *yuc1D* mutant, compared with the wild type (Fig. 3*B*). Our results indicate that the role of auxin transporters in establishing a robust auxin response gradient is specifically important already at the very first stages of cell morphology.

Defects in auxin transport lead to alteration in pavement cell shape (3). Recently, Belteton et al. questioned the involvement of PIN proteins in lobe formation, as their analysis of the *pin1-1* and triple *pin3/4/7* mutants did not reveal a significant decrease in average lobe number per cell during cotyledon development (46). We analyzed the geometry of pavement cells of mixed developmental stages in the third leaves in a variety of *pin*, *aux/lax*, and *abcb* mutants and found that the majority of the tested mutants exhibited various defects in cell area and lobe number (*SI Appendix*, Fig. S4), which correlates both with previous reports for the *pin1* mutant (3) and with findings that auxin transport and distribution regulate stomatal patterning (22). While performing cell-geometry analysis, we also noticed that some of the mutants displayed an increased number of meristemoids (marked by arrowheads in *SI Appendix*, Fig. S4*C*). Therefore, we used the dataset from the pavement cell-geometry analysis and quantified the number of meristemoids. We found that the *pin3/4/7* triple mutant, which was severely affected in pavement cell-lobe number (*SI Appendix*, Fig. S4*B*), also displayed the highest percentage of meristemoid cells (*SI Appendix*, Fig. S5*A*), which indicates that the severe disruption of auxin transport negatively affects pavement cell development.

To clarify whether the apparent discrepancy in the recent findings could be caused by differences between the tissues used, we also analyzed the size and shape of pavement cells in cotyledons of the wild type and the *pin3/4/7* triple mutant. Interestingly, like Belteton et al., we also observed decreased cell area, but no significant difference in the number of lobes in the *pin3/4/7* mutant compared with the wild type (*SI Appendix*, Fig. S5*B*), suggesting that cotyledons might use different cell shape-regulatory mechanisms from true leaves.

Taken together, our results demonstrate the coordinated and redundant roles of various auxin transporters in the fine-tuning of the dynamic auxin gradients necessary for pavement cell growth and shape acquisition.

Auxin Transporter Localization Dynamically Changes during Lobe Formation. Next, to dissect the potential roles of selected auxin transporters during formation of lobes, we examined the localization of fluorescently tagged versions of PIN3, PIN4, PIN7, AUX1, LAX1,

ABCB1, ABCB4, and ABCB19 proteins in the youngest SLGCs throughout first-lobe development. Interestingly, ABCB4-GFP (green fluorescent protein) was not visibly expressed in pavement cells, and within the leaf epidermis was only detectable in fully developed stomata (*SI Appendix*, Fig. S3*C*), which likely explains why we did not observe any pavement cell-size or -shape defects in *abcb4* mutants (*SI Appendix*, Fig. S4). Similarly, in our hands, PIN4-GFP was not expressed in pavement cells and was therefore unsuitable for quantification (*SI Appendix*, Fig. S3*D*). To investigate the localization of the other auxin transporters, we divided the anisocytic stomatal complexes into the same three stages as described earlier (Fig. 2*A*) and measured fluorescence intensity on the plasma membranes of the youngest SLGCs in each stage. We defined the SLGC perimeters beside and opposite the meristemoid or stoma as the basal and apical SLGC sides, respectively, and the other two perimeters as the lateral SLGC sides (Fig. 4 *A*, *H*, and *O*). Moreover, we then performed plasmolysis experiments to separate the plasma membranes and distinguish precisely where the fluorescently tagged proteins localized, to investigate the likely directions of auxin flow (method described in *SI Appendix*, Fig. S6).

While the distribution patterns of PIN7-GFP, LAX1-Venus, ABCB1-GFP, and ABCB19-GFP on the SLGC sides did not change much between the different stages (*SI Appendix*, Fig. S7 *A*, *B*, *E*, *F*, *I*, and *J*), some dynamic redistributions of these proteins between the adjacent membranes from one stage to another were observed (*SI Appendix*, Fig. S7 *C*, *D*, *G*, *H*, *K*, and *L*). However, the most striking localization pattern fluctuations were observed for PIN3-GFP and AUX1-Venus. At stage 1 (Fig. 4*A*), PIN3-GFP preferentially localized at the basal side of the SLGCs (Fig. 4 *B* and *D*), which actually corresponded to the membrane of the adjacent meristemoid (Fig. 4 *E* and *G*), while at the apical and lateral sides PIN3-GFP was rather localized at the SLGC membranes (Fig. 4 *E* and *G*). In contrast to PIN3-GFP, AUX1-Venus exhibited higher signal intensity at the apical and lateral sides of SLGCs (Fig. 4 *C* and *D*), where the protein was localized specifically at the adjacent cell membranes (Fig. 4 *F* and *G*). However, at the basal side, AUX1-Venus preferentially localized to the membrane of the SLGC (Fig. 4 *F* and *G*). Interestingly, after stoma development, during stages 2 (Fig. 4*H*) and 3 (Fig. 4*O*), the signal intensity of PIN3-GFP at the basal side lowered considerably (Fig. 4 *I*, *K*, *P*, and *R*), and the localization of basal PIN3-GFP changed from the adjacent cell to the SLGC membrane (Fig. 4 *L*, *N*, *S*, and *U*). Furthermore, the localization of AUX1-Venus during stage 2 and especially after lobe formation at stage 3 changed from being preferentially localized either at adjacent cell or SLGC membranes to being more equally distributed between the membranes of the different cells (Fig. 4 *J*, *K*, *M*, *N*, *Q*, *R*, *T*, and *U*).

Protein phosphorylation, as one of the posttranslational modifications, has been shown multiple times to alter PIN protein localization or its response upon various stimuli (47–49). Recently, lines with mutations mimicking constitutive dephosphorylated (PIN3-2A) or phosphorylated (PIN3-2D) status of predicted phosphorylation sites in the PIN3 protein have been published (47). We evaluated pavement cell shape, PIN3 localization at the youngest SLGC membranes, and PIN3 localization at the plasmolysis-separated plasma membranes of SLGCs and neighboring cells in these lines. We observed no effects on cell area but did observe a minor increase in the lobe number of the PIN3-2A dephosphorylated variant compared with the wild type (*SI Appendix*, Fig. S8 *A* and *B*). Examination of protein localization at the membranes of SLGCs at different stages revealed no differences compared with the wild type (*SI Appendix*, Fig. S8*C*). Plasmolysis experiments revealed only minor changes in the PIN3-2A and PIN3-2D protein distribution among the membranes of the youngest SLGC and its neighbors, which mostly resembled those of the wild type (*SI Appendix*, Fig. S8*D*). Overall, these data suggest that phosphorylation status of PIN3
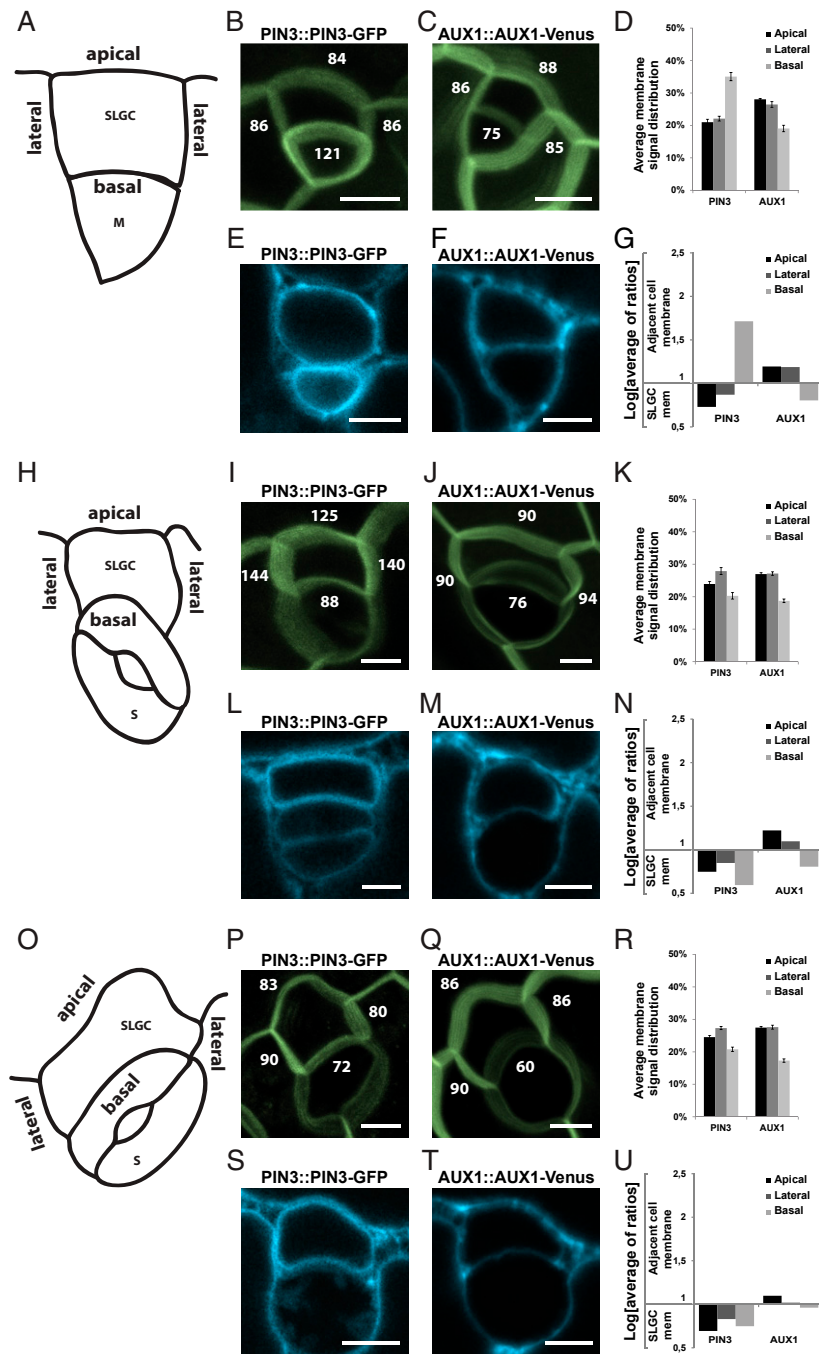
Fig. 4. Dynamic relocalization of auxin transporters during lobe formation. (*A*) Scheme representing a stage 1 SLGC with apical, basal, and lateral membranes indicated. (*B* and *C*) Maximal-intensity projections of *Z* scans of PIN3::PIN3-GFP (*B*) and AUX1::AUX1-Venus (*C*) in SLGCs from stage 1. Numbers represent quantified Venus/GFP signal intensity at the membranes. (*D*) Quantification of Venus/GFP signal distribution of PIN3::PIN3-GFP and AUX1::AUX1-Venus at the membranes of SLGCs from stage 1. (*E* and *F*) Representative single-plane images of PIN3::PIN3-GFP (*E*) and AUX1::AUX1-Venus (*F*) in SLGCs from stage 1 after plasmolysis. (*G*) Quantification of Venus/GFP signal distribution of PIN3::PIN3-GFP and AUX1::AUX1-Venus at the membranes of SLGCs from stage 1 and adjacent cells after plasmolysis. (*H*) Scheme representing a stage 2 SLGC with apical, basal, and lateral membranes indicated. (*I* and *J*) Maximal-intensity projections of *Z* scans of PIN3::PIN3-GFP (*I*) and AUX1::AUX1-Venus (*J*) in SLGCs from stage 2. Numbers represent quantified Venus/GFP signal intensity at the membranes. (*K*) Quantification of Venus/GFP signal distribution of PIN3::PIN3-GFP and AUX1::AUX1-Venus at the membranes of SLGCs from stage 2. (*L* and *M*) Representative single-plane images of PIN3::PIN3-GFP (*L*) and AUX1::AUX1-Venus (*M*) in SLGCs from stage 2 after plasmolysis. (*N*) Quantification of Venus/GFP signal distribution of PIN3::PIN3-GFP and AUX1::AUX1-Venus at the membranes of SLGCs from stage 2 and adjacent cells after plasmolysis. (*O*) Scheme representing a stage 3 SLGC with apical, basal, and lateral membranes indicated. (*P* and *Q*) Maximal-intensity projections of *Z* scans of PIN3::PIN3-GFP (*P*) and AUX1::AUX1-Venus (*Q*) in SLGCs from stage 3. Numbers represent quantified Venus/GFP signal intensity at the membranes. (*R*) Quantification of Venus/GFP signal distribution of PIN3::PIN3-GFP and AUX1::AUX1-Venus at the membranes of SLGCs from stage 3. (*S* and *T*) Representative single-plane images of PIN3::PIN3-GFP (*S*) and AUX1::AUX1-Venus (*T*) in SLGCs from stage 3 after plasmolysis. (*U*) Quantification of Venus/GFP signal distribution of PIN3::PIN3-GFP and AUX1::AUX1-Venus at the membranes of SLGCs from stage 3 and adjacent cells after plasmolysis. For all graphs, the values of two lateral membranes from one SLGC were averaged. Values from plasmolysis were log-transformed to reduce skewness; log = 1 represents an equal distribution of the signal between membranes of the SLGC and adjacent cell. Means ± SE are shown. (Scale bars, 10 μm.)

has no effect on its localization on the youngest SLGC membranes. Moreover, as shown before in *SI Appendix*, Fig. S4, alteration of only one auxin transporter does not have a major impact on pavement cell-lobe development, due to high redundancy within auxin transporters.

Together, our results suggest a directional auxin flow from the meristemoid toward the youngest neighboring SLGC via the basal membrane, coordinated by specific auxin transporter localization patterns, during stage 1 (Fig. 5*A*). Simultaneously, auxin is distributed from the SLGCs to the other, non-meristemoid, adjacent cells via the apical and lateral SLGC membranes, which might serve to regulate the specific auxin level within the SLGCs necessary at this stage (Fig. 5*A*). The removal of auxin from the meristemoid facilitates its symmetric division and stomatal formation (22), leading to stage 2, in which many of the auxin transporters have now altered their localization patterns (Fig. 5*B*). Finally, at stage 3, after lobe establishment, further relocalization of the auxin transporters likely leads to a reversal in the direction of auxin flow toward the SLGC, which might play a role in an increase of auxin levels in these cells to inhibit further lobe expansion (Fig. 5*C*). In conclusion, this work unravels the importance of remarkably dynamic auxin response gradients, tightly controlled by complicated, alternating auxin transporter localization patterns, in regulating complex plant cell shapes.

Materials and Methods

Plant Material and Growth Conditions. Before sowing, *Arabidopsis thaliana* seeds were sterilized (2 min in 70% ethanol with Tween 20, replaced with 95% ethanol for 2 min, and left until dry) and stratified at 4 °C for 48 h for uniform germination. Seedlings were grown for 14 d at 22 °C with 16 h of light per day on vertical plates of growth medium containing 1/2 Murashige and Skoog medium (MS) and 1% sucrose (Thermo Scientific) at pH 5.6 with 0.7% agar (Duchefa Biochemie). Epidermal pavement cells were analyzed on the adaxial side of the third leaf (in order of appearance: cotyledons, leaf 1, leaf 2, leaf 3), which were 6- to 8-mm-long and 4- to 5-mm-wide, from 14-d-old *Arabidopsis* plants as described previously (25). When cotyledons were analyzed, these were taken from 10-d-old *Arabidopsis* seedlings and also analyzed on the adaxial side. For performing auxin treatments, 10-d-old *Arabidopsis* seedlings possessing only first and second leaves were transferred on 1/2 MS plates containing the indicated concentrations of NAA or IAA and grown for 4 more days. Mock treatment was performed with equal volumes of solvent (dimethyl sulfoxide; Sigma-Aldrich). For pavement cell-shape analysis and live imaging, the following *Arabidopsis* lines were used: heterozygous *pin1-5* (3); *pin3-4* (50); *pin4-1* (51); *pin7-2* (50); *pin3-5/pin4-3* (22); *pin3-5/pin7-2* (52, 53); *pin4-3/pin7-2* (16); *pin3-5/pin4-3/pin7-2* (provided by Hélène S. Robert, CEITEC, Brno, Czechia); *aux1-21* (54); *aux1/lax1/lax2* (55); *abcb1, abcb19*, and *abcb1/abcb19* (38, 39); *abcb4* (40); *yuc1D* (56); DR5::Venus-NLS (15); 35S::PIP2-GFP (57); PIN3::PIN3-GFP (58); PIN4::PIN4-GFP (59); PIN7::PIN7-GFP (60); AUX1::AUX1-Venus and LAX1::LAX1-Venus (61); ABCB1::ABCB1-GFP and ABCB19::ABCB19-GFP (62); ABCB4::ABCB4-YFP (40); PIN3::PIN3-YFP, PIN3::PIN3-YFP-2A, and PIN3::PIN3-YFP-2D (47); *tir1-1* (63); *tir1-1/afb1-3/afb2-3* (64); and *afb1-2/afb2-3* and *afb4-2/afb5-5* (65). Columbia (Col-0) or Wassilewskija (Ws-0) ecotypes were used as wild-type controls in seedling-growth experiments. All mutants were genotyped before used. Genotyping primers can be found in *SI Appendix*, Table S1.

Confocal Microscopy Image Acquisition. For pavement cell-shape analysis, the third leaves from 14-d-old *Arabidopsis* seedlings were collected. Leaves were fixed for 90 min in a solution of absolute ethanol and glacial acetic acid (9:1), rehydrated in descending ethanol concentrations (70, 50, 40, 30, 20, 10%), and stored in 50% glycerol solution. Fixed leaves were treated with propidium iodide (2 μM, 1 mL; Sigma-Aldrich) for visualization of the cell outline using a confocal microscope (Zeiss; LSM 780) with a 25× differential interference contrast (DIC) 0.8 water-immersion objective. Propidium iodide was excited by a 561-nm laser line. At least four leaves and two images per leaf (50 to 100 cells per image) from the middle of the leaf blade were analyzed from each line/treatment. The experiments were repeated three times.

For pavement cell-shape analysis of cotyledons, 10-d-old seedlings were used. Cotyledons were directly stained in propidium iodide (2 μM, 1 mL; Sigma-Aldrich) and imaged using a 25× DIC 0.8 water-immersion objective mounted on a confocal microscope (Zeiss; LSM 780). Propidium iodide was excited by a 561-nm laser line. The experiment was repeated three times.

For DR5 signal distribution and auxin transporter distribution analysis, live-cell microscopy was also performed using a confocal microscope (Zeiss; LSM 780) with a 40× C-Apo 1.2 water-immersion objective. Venus or GFP was excited by 514- and 488-nm laser lines, respectively. Leaves were treated with propidium iodide (2 μM, 1 mL; Sigma-Aldrich) for visualization of the cell outline. The acquired images were analyzed using ImageJ (NIH; http://rsb.info.nih.gov/ij). Quantification of DR5::Venus-NLS signal and auxin transporter localization on membranes of SLGCs was performed on maximal-intensity projections of Z scans. The DR5 gradients were only analyzed in developed spirals consisting of a meristemoid/stoma and three SLGCs, in which the ascending or descending pattern must be followed throughout all these cells. The experiment was repeated three times.

Plasmolysis was performed using a 1 M NaCl solution, in which the leaves were incubated for 5 min. The images were acquired analogously as for auxin transporter distribution. The quantification was performed by separate analysis of different slices of Z scans as described in *SI Appendix*, Fig. S6. The experiment was repeated three times.

Pavement Cell-Size and -Shape Analysis. The area and lobe number of pavement cells of mixed developmental stages were measured as follows. Confocal microscopy raw images from four different third leaves were preprocessed in order to enhance cell-wall signal using the following ImageJ functions: *subtract background* and *enhance contrast*. Images were segmented using CellSeT (66). Stomata were then filled with background. Area was measured for each cell using the *analyze particles* function in ImageJ. Lobe number was estimated automatically using the *skeletonize* function and the plugin *analyze skeleton*. Cell-area values were log-transformed to reduce skewness and statistics was performed using the Wilcoxon test in R software. Experiments were always repeated three times in three independent biological replicates, which showed the same patterns. Only the data from one representative experiment are presented in the figures, and *n* values in the figure legends represent the total number of cells analyzed in that one particular experiment.

SLGC Lobe Outgrowth Angle Quantification. Nonlobed SLGCs were considered as cells with an outgrowth ratio <1:1 (<10%) and lobed SLGCs as cells with an outgrowth ratio >1:1 (>10%). Outgrowth ratio was calculated by dividing the membrane length by the Euclidean point distance (the minimal distance between two cell corners of the membrane where the lobe will be/has formed). The positioning of the first SLGC lobe was analyzed by measuring the angle between the highest point of the lobe (tip) and the center of the neighboring stoma.

Data Availability. All data underlying the study are available in the paper or *SI Appendix*, and all material discussed in the paper will be made available to readers upon request.
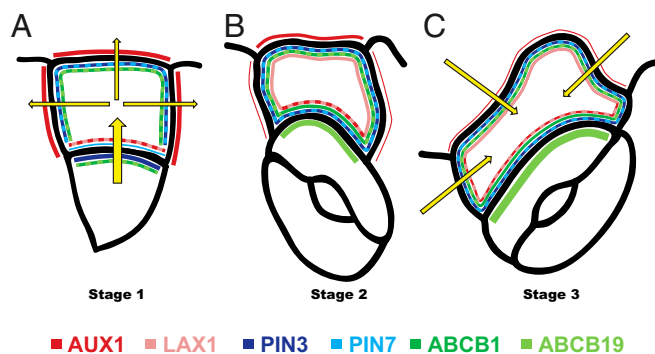
Fig. 5. Model representing auxin transporter distribution at different membranes of SLGCs and adjacent cells. (*A*) Distribution of auxin transporters at stage 1. (*B*) Distribution of auxin transporters at stage 2. (*C*) Distribution of auxin transporters at stage 3. Line thickness represents transporter abundance. Yellow arrows represent auxin flow.

1. M. Geisler, J. Nadeau, F. D. Sack, Oriented asymmetric divisions that generate the stomatal spacing pattern in *Arabidopsis* are disrupted by the too many mouths mutation. *Plant Cell* **12**, 2075–2086 (2000).

2. U. Von Groll, D. Berger, T. Altmann, The subtilisin-like serine protease SDD1 mediates cell-to-cell signaling during *Arabidopsis* stomatal development. *Plant Cell* **14**, 1527–1539 (2002).

3. T. Xu *et al.*, Cell surface- and rho GTPase-based auxin signaling controls cellular interdigitation in *Arabidopsis*. *Cell* **143**, 99–110 (2010).

4. X. Guo *et al.*, TYPE-ONE PROTEIN PHOSPHATASE4 regulates pavement cell interdigitation by modulating PIN-FORMED1 polarity and trafficking in *Arabidopsis*. *Plant Physiol.* **167**, 1058–1075 (2015).

5. P. Grones *et al.*, Auxin-binding pocket of ABP1 is crucial for its gain-of-function cellular and developmental roles. *J. Exp. Bot.* **66**, 5055–5065 (2015).

6. R. J. Pitts, A. Cernac, M. Estelle, Auxin and ethylene promote root hair elongation in *Arabidopsis*. *Plant J.* **16**, 553–560 (1998).

7. A. Rahman *et al.*, Auxin and ethylene response interactions during *Arabidopsis* root hair development dissected by auxin influx modulators. *Plant Physiol.* **130**, 1908–1917 (2002).

8. T. Ishida, T. Kurata, K. Okada, T. Wada, A genetic regulatory network in the development of trichomes and root hairs. *Annu. Rev. Plant Biol.* **59**, 365–386 (2008).

9. B. Péret *et al.*, *Arabidopsis* lateral root development: An emerging story. *Trends Plant Sci.* **14**, 399–408 (2009).

10. C. Dubreuil, X. Jin, A. Grönlund, U. Fischer, A local auxin gradient regulates root cap self-renewal and size homeostasis. *Curr. Biol.* **28**, 2581–2587.e3 (2018).

11. D. Weijers, D. Wagner, Transcriptional responses to the auxin hormone. *Annu. Rev. Plant Biol.* **67**, 539–574 (2016).

12. L. I. A. Calderón Villalobos *et al.*, A combinatorial TIR1/AFB-Aux/IAA co-receptor system for differential sensing of auxin. *Nat. Chem. Biol.* **8**, 477–485 (2012).

13. S. Lee *et al.*, Defining binding efficiency and specificity of auxins for SCF(TIR1/AFB)-Aux/IAA co-receptor complex formation. *ACS Chem. Biol.* **9**, 673–682 (2014).

14. Y. Shimizu-Mitao, T. Kakimoto, Auxin sensitivities of all *Arabidopsis* Aux/IAAs for degradation in the presence of every TIR1/AFB. *Plant Cell Physiol.* **55**, 1450–1459 (2014).

15. M. G. Heisler *et al.*, Patterns of auxin transport and gene expression during primordium development revealed by live imaging of the *Arabidopsis* inflorescence meristem. *Curr. Biol.* **15**, 1899–1911 (2005).

16. E. Benková *et al.*, Local, efflux-dependent auxin gradients as a common module for plant organ formation. *Cell* **115**, 591–602 (2003).

17. I. De Smet *et al.*, Auxin-dependent regulation of lateral root positioning in the basal meristem of *Arabidopsis*. *Development* **134**, 681–690 (2007).

18. M. A. Moreno-Risueno *et al.*, Oscillating gene expression determines competence for periodic *Arabidopsis* root branching. *Science* **329**, 1306–1311 (2010).

19. T. Vernoux *et al.*, The auxin signalling network translates dynamic input into robust patterning at the shoot apex. *Mol. Syst. Biol.* **7**, 508 (2011).

20. G. Brunoud *et al.*, A novel sensor to map auxin response and distribution at high spatio-temporal resolution. *Nature* **482**, 103–106 (2012).

21. J. Yang *et al.*, Dynamic regulation of auxin response during rice development revealed by newly established hormone biosensor markers. *Front Plant Sci* **8**, 256 (2017).

22. J. Le *et al.*, Auxin transport and activity regulate stomatal patterning and development. *Nat. Commun.* **5**, 3090 (2014).

23. M. Fujita *et al.*, The anisotropy1 D604N mutation in the *Arabidopsis* cellulose synthase1 catalytic domain reduces cell wall crystallinity and the velocity of cellulose synthase complexes. *Plant Physiol.* **162**, 74–85 (2013).

24. Y. Fu, H. Li, Z. Yang, The ROP2 GTPase controls the formation of cortical fine F-actin and the early phase of directional cell expansion during *Arabidopsis* organogenesis. *Plant Cell* **14**, 777–794 (2002).

25. M. Majda *et al.*, Mechanochemical polarization of contiguous cell walls shapes plant pavement cells. *Dev. Cell* **43**, 290–304.e4 (2017).

26. D. Reinhardt *et al.*, Regulation of phyllotaxis by polar auxin transport. *Nature* **426**, 255–260 (2003).

27. C. Kuhlemeier, Phyllotaxis. *Trends Plant Sci.* **12**, 143–150 (2007).

28. Y. Deb, D. Marti, M. Frenz, C. Kuhlemeier, D. Reinhardt, Phyllotaxis involves auxin drainage through leaf primordia. *Development* **142**, 1992–2001 (2015).

29. W. Xuan *et al.*, Root cap-derived auxin pre-patterns the longitudinal axis of the *Arabidopsis* root. *Curr. Biol.* **25**, 1381–1388 (2015).

30. D. Reinhardt, T. Mandel, C. Kuhlemeier, Auxin regulates the initiation and radial position of plant lateral organs. *Plant Cell* **12**, 507–518 (2000).

31. S. Yoshida *et al.*, Genetic control of plant development by overriding a geometric division rule. *Dev. Cell* **29**, 75–87 (2014).

32. K. Ljung, R. P. Bhalerao, G. Sandberg, Sites and homeostatic control of auxin biosynthesis in *Arabidopsis* during vegetative growth. *Plant J.* **28**, 465–474 (2001).

33. E. M. Kramer, E. M. Ackelsberg, Auxin metabolism rates and implications for plant development. *Front Plant Sci* **6**, 150 (2015).

34. M. Adamowski, J. Friml, PIN-dependent auxin transport: Action, regulation, and evolution. *Plant Cell* **27**, 20–32 (2015).

35. M. J. Bennett *et al.*, *Arabidopsis* AUX1 gene: A permease-like regulator of root gravitropism. *Science* **273**, 948–950 (1996).

36. R. Swarup *et al.*, Root gravitropism requires lateral root cap and epidermal cells for transport and response to a mobile auxin signal. *Nat. Cell Biol.* **7**, 1057–1065 (2005).

37. B. Péret *et al.*, AUX/LAX genes encode a family of auxin influx transporters that perform distinct functions during *Arabidopsis* development. *Plant Cell* **24**, 2874–2885 (2012).

38. B. Noh, A. S. Murphy, E. P. Spalding, Multidrug resistance-like genes of *Arabidopsis* required for auxin transport and auxin-mediated development. *Plant Cell* **13**, 2441–2454 (2001).

39. M. Geisler *et al.*, TWISTED DWARF1, a unique plasma membrane-anchored immunophilin-like protein, interacts with *Arabidopsis* multidrug resistance-like transporters AtPGP1 and AtPGP19. *Mol. Biol. Cell* **14**, 4238–4249 (2003).

40. K. Terasaka *et al.*, PGP4, an ATP binding cassette P-glycoprotein, catalyzes auxin transport in *Arabidopsis thaliana* roots. *Plant Cell* **17**, 2922–2939 (2005).

41. B. Titapiwatanakun *et al.*, ABCB19/PGP19 stabilises PIN1 in membrane microdomains in *Arabidopsis*. *Plant J.* **57**, 27–44 (2009).

42. M. Geisler *et al.*, Cellular efflux of auxin catalyzed by the *Arabidopsis* MDR/PGP transporter AtPGP1. *Plant J.* **44**, 179–194 (2005).

43. A. Kasprzewska *et al.*, Auxin influx importers modulate serration along the leaf margin. *Plant J.* **83**, 705–718 (2015).

44. S. Nagawa *et al.*, ROP GTPase-dependent actin microfilaments promote PIN1 polarization by localized inhibition of clathrin-dependent endocytosis. *PLoS Biol.* **10**, e1001299 (2012).

45. X. Chen, J. Friml, Rho-GTPase-regulated vesicle trafficking in plant cell polarity. *Biochem. Soc. Trans.* **42**, 212–218 (2014).

46. S. A. Belteton, M. G. Sawchuk, B. S. Donohoe, E. Scarpella, D. B. Szymanski, Reassessing the roles of PIN proteins and anticlinal microtubules during pavement cell morphogenesis. *Plant Physiol.* **176**, 432–449 (2018).

47. P. Grones *et al.*, PID/WAG-mediated phosphorylation of the *Arabidopsis* PIN3 auxin transporter mediates polarity switches during gravitropism. *Sci. Rep.* **8**, 10279 (2018).

48. P. Dhonukshe *et al.*, Plasma membrane-bound AGC3 kinases phosphorylate PIN auxin carriers at TPRXS(N/S) motifs to direct apical PIN recycling. *Development* **137**, 3245–3255 (2010).

49. B. Weller *et al.*, Dynamic PIN-FORMED auxin efflux carrier phosphorylation at the plasma membrane controls auxin efflux-dependent growth. *Proc. Natl. Acad. Sci. U.S.A.* **114**, E887–E896 (2017).

50. J. Friml *et al.*, Efflux-dependent auxin gradients establish the apical-basal axis of *Arabidopsis*. *Nature* **426**, 147–153 (2003).

51. J. Friml *et al.*, AtPIN4 mediates sink-driven auxin gradients and root patterning in *Arabidopsis*. *Cell* **108**, 661–673 (2002).

52. J. Kleine-Vehn *et al.*, Gravity-induced PIN transcytosis for polarization of auxin fluxes in gravity-sensing root cells. *Proc. Natl. Acad. Sci. U.S.A.* **107**, 22344–22349 (2010).

53. K. Haga, T. Sakai, PIN auxin efflux carriers are necessary for pulse-induced but not continuous light-induced phototropism in *Arabidopsis*. *Plant Physiol.* **160**, 763–776 (2012).

54. A. Marchant, M. J. Bennett, The *Arabidopsis* AUX1 gene: A model system to study mRNA processing in plants. *Plant Mol. Biol.* **36**, 463–471 (1998).

55. K. Swarup *et al.*, The auxin influx carrier LAX3 promotes lateral root emergence. *Nat. Cell Biol.* **10**, 946–954 (2008).

56. Y. Zhao *et al.*, A role for flavin monooxygenase-like enzymes in auxin biosynthesis. *Science* **291**, 306–309 (2001).

57. S. R. Cutler, D. W. Ehrhardt, J. S. Griffitts, C. R. Somerville, Random GFP:cDNA fusions enable visualization of subcellular structures in cells of *Arabidopsis* at a high frequency. *Proc. Natl. Acad. Sci. U.S.A.* **97**, 3718–3723 (2000).

58. P. Zádníková *et al.*, Role of PIN-mediated auxin efflux in apical hook development of *Arabidopsis thaliana*. *Development* **137**, 607–617 (2010).

59. A. Vieten *et al.*, Functional redundancy of PIN proteins is accompanied by auxin-dependent cross-regulation of PIN expression. *Development* **132**, 4521–4531 (2005).

60. I. Blilou *et al.*, The PIN auxin efflux facilitator network controls growth and patterning in *Arabidopsis* roots. *Nature* **433**, 39–44 (2005).

61. N. Fàbregas *et al.*, Auxin influx carriers control vascular patterning and xylem differentiation in *Arabidopsis thaliana*. *PLoS Genet.* **11**, e1005183 (2015).

62. J. Mravec *et al.*, Interaction of PIN and PGP transport mechanisms in auxin distribution-dependent development. *Development* **135**, 3345–3354 (2008).

63. M. Ruegger *et al.*, The TIR1 protein of *Arabidopsis* functions in auxin response and is related to human SKP2 and yeast grr1p. *Genes Dev.* **12**, 198–207 (1998).

64. G. Parry *et al.*, Complex regulation of the TIR1/AFB family of auxin receptors. *Proc. Natl. Acad. Sci. U.S.A.* **106**, 22540–22545 (2009).

65. K. Greenham *et al.*, The AFB4 auxin receptor is a negative regulator of auxin signaling in seedlings. *Curr. Biol.* **21**, 520–525 (2011). Retraction in: *Curr. Biol.* **25**, 819 (2015).

66. M. P. Pound, A. P. French, D. M. Wells, M. J. Bennett, T. P. Pridmore, CellSeT: Novel software to extract and analyze structured networks of plant cells from confocal images. *Plant Cell* **24**, 1353–1361 (2012).